ELSEVIER

Water transport coefficient distribution through the membrane in a polymer electrolyte fuel cell

Fuqiang Liu [a,1], Guoqiang Lu [b], Chao-Yang Wang [a,b,*]

[a] Department of Materials Science and Engineering, Electrochemical Engine Center (ECEC), The Pennsylvania State University,
University Park, PA 16802, United States
[b] Department of Mechanical and Nuclear Engineering, Electrochemical Engine Center (ECEC), The Pennsylvania State University,
University Park, PA 16802, United States

Abstract

The net water transport coefficient through the membrane, defined as the ratio of the net water flux from the anode to cathode to the protonic flux, is used as a quantitative measure of water management in a polymer electrolyte fuel cell (PEFC). In this paper we report on experimental measurements of the net water transport coefficient distribution for the first time. This is accomplished by making simultaneous current and species distribution measurements along the flow channel of an instrumented PEFC via a multi-channel potentiostat and two micro gas chromatographs. The net water transport coefficient profile along the flow channels is then determined by a control-volume analysis under various anode and cathode inlet relative humidity (RH) at 80 °C and 2 atm. It is found that the local current density is dominated by the membrane hydration and that the gas RH has a large effect on water transport through the membrane. Very small or negative water transport coefficients are obtained, indicating strong water back diffusion through the 30 μm Gore-Select® membrane used in this study.
© 2006 Elsevier B.V. All rights reserved.

Keywords: Water transport; Fuel cells; Membranes; Experimental measurements; Back diffusion

1. Introduction

The operation of polymer electrolyte fuel cells (PEFCs) requires delicate water management to achieve high performance and longevity. The currently available fluorinated membranes such as Nafion require water in order to exhibit high proton conductivity. However, if too much water is present in the cell, the pores in the catalyst layer (CL) and gas diffusion layer (GDL) are filled with liquid water, resulting in cathode flooding and mass transport loss. Therefore, understanding water transport in a PEFC, particularly through the polymer membrane, is of great importance to avoid either membrane dehydration or cathode flooding, as well as to guide the optimization of materials and membrane–electrode assemblies (MEA).

Water is transported through the membrane from the anode to cathode via electro-osmotic drag that is directly proportional to the current density. The water transported and generated at the cathode creates a high water concentration or a high hydraulic pressure in the cathode catalyst layer, driving the water back-transport from the cathode to anode either through a diffusion mechanism [1–3] or a hydraulic permeation mechanism [4–6]. The net water transport is thus a net result of electro-osmosis, back diffusion, and hydraulic permeation across the membrane and is quantified in terms of the net water transport coefficient, $\alpha = N_{H_2O}/N_{H^+}$. The magnitude and spatial distribution of α are very important for the design of innovative water management strategies in PEFCs.

Understanding water transport and balance in PEFCs has been a focus of recent research. Different models were developed to describe various water transport mechanisms in the membranes. Springer et al. [1] predicted the net water transport coefficient across the membrane based on a diffusion model. Nguyen and White [3] used a combined heat and water diffusion model to predict the osmotic drag coefficient and α along the flow channels. Bernardi and Verbrugge [4] developed a

* Corresponding author at: 338A Reber Building, The Pennsylvania State University, University Park, PA 16802, United States. Tel.: +1 814 863 4762; fax: +1 814 863 4848.
  E-mail address: cxw31@psu.edu (C.-Y. Wang).
[1] Present address: United Technologies Research Center, 411 Silver Lane, East Hartford, CT 06108, United States.

hydraulic permeation model and analyzed the effects of different operating conditions on water balance in fuel cells. Fuller and Newman [7] simulated water transport in a PEFC using a concentrated solution theory and predicted the water distribution in the membrane and the net water transport coefficient. To date, the multiple mechanisms of water transport across the membrane still remain unclear, and the modeling results need experimental validation. Experimentally, overall water balance has been commonly performed in fuel cells by collecting water from the fuel cell effluents through ice traps or other methods [8–10]. However, the net water transport coefficient averaged over the entire active area of a PEFC is insufficient for the basic understanding of localized flooding and degradation occurring in a PEFC. Indeed, α varies greatly along the flow stream, as a combined result of variations in membrane hydration, local current density, and local water concentration in both anode and cathode gas streams.

The objective of this paper is to present a novel method to determine α-distribution along the flow direction by simultaneous measurements of current density and species concentration distributions in a segmented test cell. Distribution data will be shown for a range of low-humidity conditions at the anode and cathode that are representative of present automotive PEFC engines. The α-distribution data presented in this work are expected to be useful for the design of water management systems as well as for validation and improvement of next-generation fuel cell models [11].

2. Experimental

An instrumented cell with 10 segmented sub-cells was used to measure the current density and species distributions. The total active area of the instrumented cell is 6 cm^2 consisting of three parallel straight channels of 10 cm long. A Lexan polycarbonate plate is used to electrically isolate the flowfield/current collectors. Ten stainless steel segments are embedded in the Lexan plate, separated by tiny pieces of Teflon sheet used to maintain a continuous flowfield of three-pass straight channels. Fig. 1 gives the dimension of each stainless steel segment. Three straight-flow channels are machined in the surface, each with the dept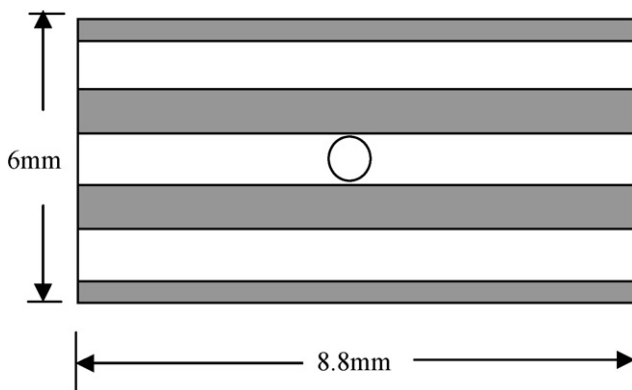h of 0.5 mm and width of 1 mm. The land separating two neighboring channels is 1 mm wide. In the center of each stainless steel segment, a through hole with a diameter of 1 mm is soldered with a stainless steel hollow tube or a pin designed for two functions. The tube wall conducts the electric current, and the inner hole inside each pin is used to extract gas samples for concentration measurement. Both the pins and segments are gold-plated in order to minimize the contact resistance and to prevent corrosion. A stainless steel plate is added on the outside of the Lexan plate for mechanical support, and an electrical heater is attached on the plate to control the cell temperature. The gas streams along the anode and cathode channels are arranged in co-flow. Calculated from the inlet, the fractional locations of segment centers are $x/L = 0.05, 0.15, 0.25, 0.35, 0.45, 0.55, 0.65, 0.75, 0.85$ and 0.95, respectively.

The experimental setup has been detailed in the previous publications of Wang group at ECEC [12–14] and thus is not repeated here. The 10 segments forming the sub-cells were connected to 10 independent channels of a potentiostat for current distribution measurements under a prescribed cell voltage. Under steady-state operation with constant voltage control, two microgas chromatographs (GC) from Agilent were used to measure the species concentration in the anode and cathode flows, respectively. The sampling ports in the instrumented cell are connected to a multi-port micro-electric actuator (Valco), and then to the inlet of each GC, which is heated at 130 °C to prevent water condensation. The actuator can automatically switch the connection from one sampling port to another with the inlet of the MicroGC.

A membrane electrode assembly (MEA) based on a 30-μm thick Gore-Select® membrane with an active area of 6 cm^2 is used in the present study. Hydrophobic carbon cloth with a pre-coated micro-porous layer is used as GDL, without segmentation. The cell is operated under different anode and cathode inlet RH at 80 °C and 2 atm (absolute pressure) on both sides. Hydrogen and air with different inlet RH are fed to the anode and cathode, respectively, in co-flow. The flow stoichiometry for the anode and cathode was $\xi_a/\xi_c = 2/2$ at 1 A/cm^2, i.e. constant flowrates equivalent to 2 A/cm^2.

3. Determination of α-distribution

The molar flowrates of hydrogen $N_{H_2}(y)$ and water $N_{H_2O}(y)$ along the anode channel length y vary due to the hydrogen oxidation reaction and net water transport through the membrane, respectively. It thus follows that

$$\frac{dN_{H_2}(y)}{dy} = -b\frac{I(y)}{2F} \tag{1}$$

$$\frac{dN_{H_2O}(y)}{dy} = -b\frac{\alpha(y)I(y)}{F} \tag{2}$$

where b is the width of the flow channel and F is the Faraday constant. The current density $I(y)$ and net water transport coefficient $\alpha(y)$ vary along the channel length with the membrane conductivity and water uptake. Hydrogen crossover through the

Fig. 1. Schematic of the segment where the gray areas are lands and the hole at the center is for gas sampling.

6mm

8.8mm

membrane is negligible in Eq. (1); thus one has

$$N_{H_2}(y) = N_{H_2}^{in} - \frac{b}{2F} \int_0^y I(y)\, dy \tag{3}$$

where $N_{H_2}^{in}$ is the inlet hydrogen molar flowrate. If there is no liquid water condensed in the flow stream, $N_{H_2}(y)$ and $N_{H_2O}(y)$ can be related by

$$N_{H_2O}(y) = N_{H_2}(y) \frac{x_{H_2O}^a(y)}{x_{H_2}(y)} \tag{4}$$

where $x_{H_2}(y)$ and $x_{H_2O}^a(y)$ are the hydrogen and water molar fractions along the anode channel length. Substituting Eqs. (3) and (4) into Eq. (2), $\alpha(y)$ can be expressed as

$$\alpha(y) = -\frac{F}{bI(y)} \frac{d}{dy} \left\{ \left(N_{H_2}^{in} - \frac{b}{2F} \int_0^y I(y)\, dy \right) \frac{x_{H_2O}^a(y)}{x_{H_2}(y)} \right\} \tag{5}$$

or

$$\alpha(y) = -\frac{F \left(N_{H_2}^{in} - (b/2F) \int_0^y I(y)\, dy \right)}{bI(y)} \frac{d}{dy} \left(\frac{x_{H_2O}^a(y)}{x_{H_2}(y)} \right)$$
$$+ \frac{x_{H_2O}^a(y)}{2x_{H_2}(y)} \tag{6}$$

The derivation of Eq. (6) is given in Appendix A. The fact that $x_{H_2O}^a(y) + x_{H_2}(y) = 1$ may further simplify Eq. (6) by eliminating either $x_{H_2O}^a(y)$ or $x_{H_2}(y)$. The distribution of $\alpha(y)$ along the channel is determined by Eq. (6). The variables, $I(y)$, $x_{H_2}(y)$ and $x_{H_2O}^a(y)$, at different fractional locations can be experimentally determined by simultaneous current density and species distribution measurements. Continuous functions of $I(y)$, $x_{H_2}(y)$ and $x_{H_2O}^a(y)$ are obtained by third-order polynomial fitting of the experimental data points with correlation coefficients greater than 0.98, which are then used to calculate $d(x_{H_2O}^a(y)/x_{H_2}(y))/dy$ and $\int_0^y I(y)\, dy$. Note that the α-distribution through the membrane can be alternatively obtained from the cathode species distribution data along with current distribution data, albeit requiring higher measurement accuracy of cathode water because the cathode produces much water; see Ref. [23] for more discussions.

4. Results and discussion

A set of simultaneous current density and species distribution measurements along the flow channel are conducted at 0.6 V and 2 atm, under three different anode and cathode inlet RH: (1) $RH_a = 42\%$, $RH_c = 42\%$; (2) $RH_a = 0\%$, $RH_c = 42\%$; (3) $RH_a = 42\%$, $RH_c = 0\%$. The humidity RH = 42% corresponds to a dew point of 60 °C for the cell temperature of 80 °C.

Fig. 2 shows the current density profile along the flow path at 0.6 V cell voltage and various combinations of anode and cathode inlet RH. Minimum current densities are observed at the inlet, and increase monotonically toward the outlet as the membrane takes up water. Cell operation at the same RH = 42% on both sides in Case 1 yields the best performance, while with either dry anode or cathode inlet, Case 2 or 3 achieves only about
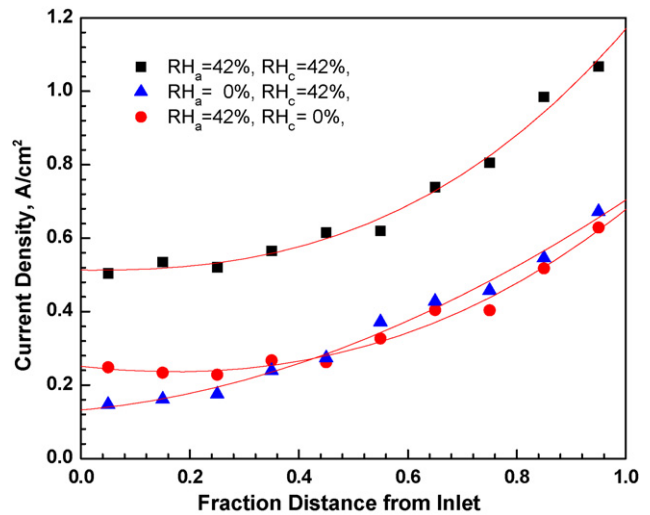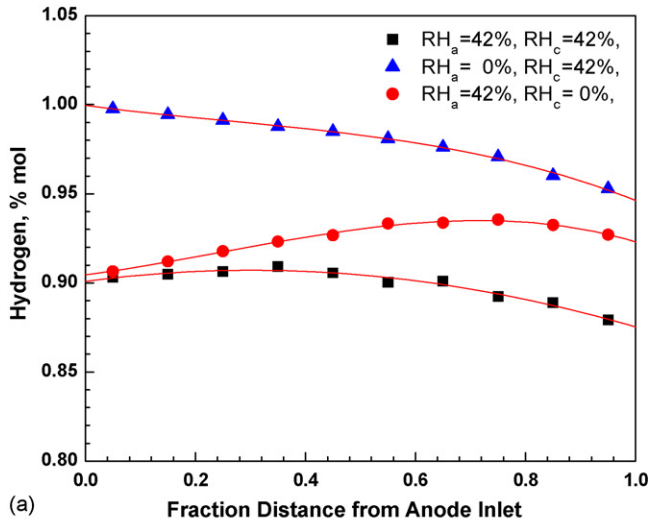

Fig. 2. Current density distribution along the flow direction for a co-flow H_2/air fuel cell with $\xi_a = 2$ at 1 A/cm^2 and $\xi_c = 2$ at 1 A/cm^2 at 2 atm and 0.6 V. The lines are the third-order polynomial fitting results.
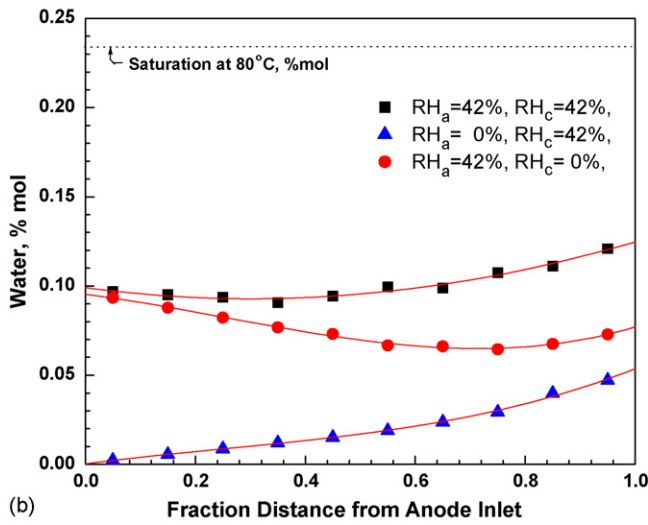
half of the current density in Case 1. Case 2 exhibits the smallest current density at the inlet. However, the current density increases very rapidly and exceeds that of Case 3 at the outlet, probably because the membrane gains water more quickly in Case 2 by the enhanced back diffusion from the cathode to anode.

Fig. 3 shows the distributions of hydrogen and water concentrations along the anode flow path. For Case 2 with the dry anode inlet, the water concentration increases quite linearly along the flow path, indicating a strong water back diffusion from the cathode to compensate for the electro-osmotic drag. For the other two cases, the water concentrations first decrease slightly, probably due to electro-osmotic drag that increases with the current density along the path. After experiencing minimum points, i.e. at $x/L = 0.35$ for Case 1 and $x/L = 0.75$ for Case 3, water concentrations then increase due to enhanced back diffusion of water from the cathode to anode when there is sufficient water buildup in the cathode catalyst layer. The hydrogen concentration distributions along the anode channel vary according to the water concentration in this binary system.

Fig. 4 displays the oxygen and water concentration profiles along the cathode flow path at 0.6 V cell voltage. Case 1 shows a larger oxygen consumption rate, consistent with its superior performance. It is believed that better hydration of the ionomer in the catalyst layer and membrane results in improved activation and proton conductivity. The water concentration at the exit is 16.5 mol%, still below the saturation value (i.e. 23.3 mol% at 80 °C and 2 atm). In Case 2, the dry anode inlet results in enhanced water back diffusion from cathode to anode which is high enough to offset the water generated by ORR and transported by the electro-osmotic drag. The combination of these three factors yields a uniform profile of water concentration in the cathode gas channel. In Case 3 with a dry cathode inlet, the oxygen and water concentration profiles are quite linear, reaching 17.6 mol% and 8.9 mol%, respectively, at the exit.
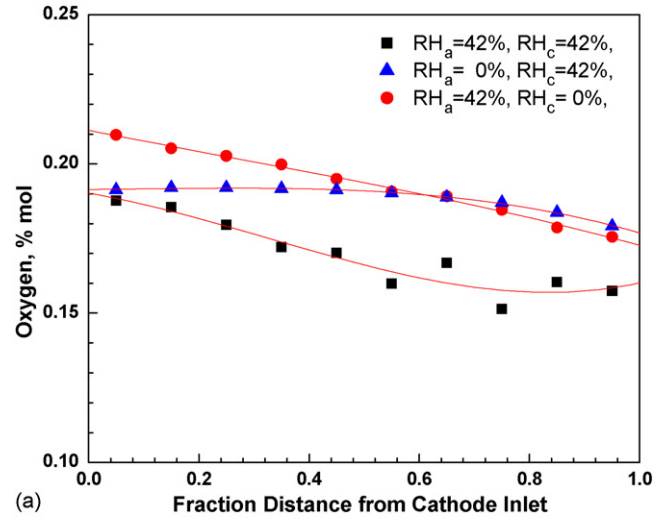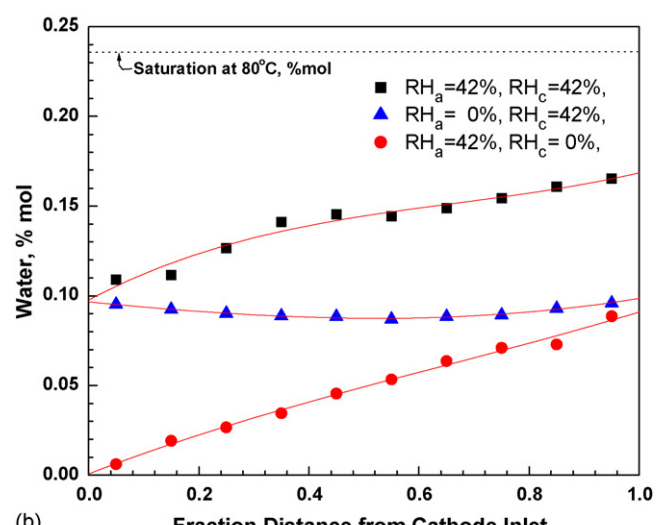
Fig. 3. (a) Hydrogen and (b) water concentration distributions along the anode flow path for a co-flow H_2/air fuel cell with $\xi_a = 2$ at 1 A/cm^2 and $\xi_c = 2$ at 1 A/cm^2 at 2 atm and 0.6 V. The lines are the third-order polynomial fitting.

Fig. 4. (a) Oxygen and (b) water concentration distributions along the cathode flow path for a co-flow H_2/air fuel cell with $\xi_a = 2$ at 1 A/cm^2 and $\xi_c = 2$ at 1 A/cm^2 at 2 atm and 0.6 V. The lines are the third-order polynomial fitting.

Both the anode and cathode exit gases are unsaturated as indicated in Figs. 3b and 4b, making Eq. (6) valid for determination of net water transport coefficient distribution across the membrane. Fig. 5 shows the α-distribution along the flow path calculated by Eq. (6) using the anode data, and numerical values of α are also listed in Table 1. Small positive α values are observed when both anode and cathode inlets are partially humidified at the same RH = 42% (i.e. Case 1). The net water transport coefficient drops from 0.14 to zero in the first half of the flow channel length and levels off in the second half. When the anode inlet is dry in Case 2, more water is transported from the cathode to anode, resulting in negative α ranging from -0.249 at the inlet to -0.125 at the outlet. For Case 3 with dry cathode inlet, after an initial plateau in the beginning 30% of the channel, α drops dramatically in the remaining section where the cathode catalyst layer builds up sufficient water concentration to facilitate water back diffusion.

Ignoring hydraulic permeation due to water activity, generally smaller than unity in the range of this study, the net water transport coefficient α can be mathematically expressed as

$$\alpha = n_d - \frac{F}{I} D \frac{\rho_m(\lambda_c - \lambda_a)}{\delta_m EW} \tag{7}$$

Table 1
α-Distribution data as shown in Fig. 5

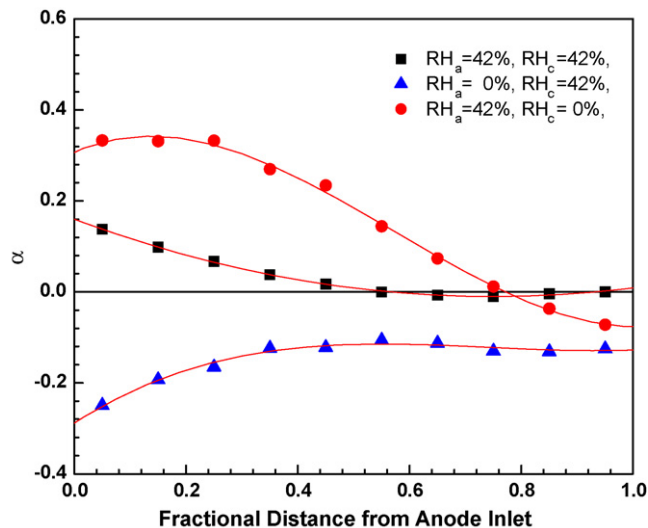| Fraction distance from anode inlet, y	Case 1	Case 2	Case 3
0.05	0.137	-0.249	0.333
0.15	0.098	-0.193	0.332
0.25	0.067	-0.165	0.332
0.35	0.037	-0.124	0.270
0.45	0.017	-0.122	0.234
0.55	0.000	-0.106	0.144
0.65	-0.007	-0.113	0.074
0.75	-0.011	-0.130	0.012
0.85	-0.004	-0.131	-0.037
0.95	0.000	-0.125	-0.072

Fig. 5. The net water transport coefficient distribution for a co-flow H_2/air fuel cell with $\xi_a = 2$ at 1 A/cm^2 and $\xi_c = 2$ at 1 A/cm^2 at 2 atm and 0.6 V. The lines are the third-order polynomial fitting.

Fig. 6. Cathode and anode water concentration difference, $c_{H_2O}^c - c_{H_2O}^a$, along the flow path for different cases: (1) $RH_a = 42\%$, $RH_c = 42\%$; (2) $RH_a = 0\%$, $RH_c = 42\%$; (3) $RH_a = 42\%$, $RH_c = 0\%$.

where n_d is the electro-osmotic drag coefficient of water, D the water diffusivity in the membrane, δ_m the membrane thickness, λ the water content $[H_2O]/[SO_3^-]$ accompanying with the sulfonate group in Nafion, EW the equivalent weight (weight of dry polymer resin per mole SO_3^- group), and ρ_m is the density of the ionomeric membrane. The α values measured in this work are much smaller than the pure electro-osmotic drag number reported for Nafion membranes with the equivalent weight of 1100 [15–19] and Gore-Select® membranes with the equivalent weight of 950 [20]. The electro-osmotic drag coefficient varies within a wide range, depending on the degree of membrane hydration, from 2 to 3 at room temperature in a Nafion 117 membrane in contact with liquid water. When equilibrated with water vapor, a water drag coefficient of unity is found independent of water content in the membrane [21], possibly indicating that the drag coefficient is determined by the same proton transport mechanisms for all fluorinated membranes [22]. The electro-osmotic drag coefficient of Gore-Select® membranes was recently measured to be approximately unity in the water activity range of 0.4–0.95 [20].

With roughly unity electro-osmotic drag coefficient, the α-distribution is controlled principally by the concentration difference for water diffusion according to Eq. (7). In Fig. 6 the water concentration difference between the cathode and anode gas channels, $(c_{H_2O}^c - c_{H_2O}^a)$, is plotted as a function of the fractional distance along the flow path for the three cases. Indeed, the trend correlates well with the α-distributions shown in Fig. 5 (or more precisely $-\alpha$ as α represents the water flux from the anode to cathode). Thus the value of $(c_{H_2O}^c - c_{H_2O}^a)$ appears to be a good indicator of the water concentration gradient across the membrane, i.e. $(\lambda_c - \lambda_a)$. In Fig. 6, despite different combinations of anode and cathode inlet humidity, $(c_{H_2O}^c - c_{H_2O}^a)$ converges to positive values near the fuel cell exit, opposing the water loss from the anode via electro-osmosis. At the same time, the higher water concentration in the gas streams near the exit leads to better membrane hydration and increased water diffu-
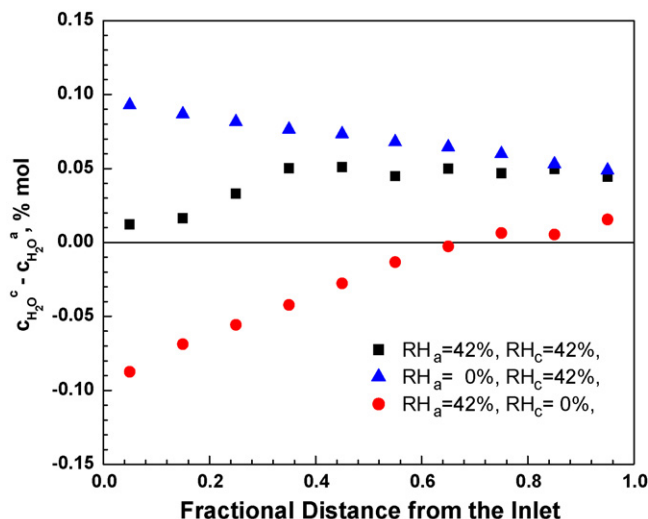
sivity through the membrane, resulting in higher current density and greater water back diffusion.

5. Conclusion

Spatial distribution of the net water transport coefficient through the membrane along the flow direction has been determined by simultaneously measuring local current density and water concentrations in an instrumented PEFC. Under low anode and cathode inlet RH, the local current density is dominated by membrane hydration and increases monotonically from the inlet toward the outlet as the membrane takes up water. The water concentration and α profiles result from delicate balance between the electro-osmotic drag and back diffusion from the cathode to anode. A dry anode inlet promotes water back diffusion and yields negative α, whereas a dry cathode inlet gives rise to negative α only towards the exit of the fuel cell where the cathode stream accumulates enough water from ORR for back diffusion. When both anode and cathode have the same inlet RH = 42%, α decreases slowly from 0.14 at the inlet to zero at the outlet.

Appendix A

By rearranging the right-hand side of Eq. (5), one has

$$\alpha(y) = -\frac{F}{bI(y)} \frac{d}{dy}\left(N_{H_2}^{in} \frac{x_{H_2O}^a(y)}{x_{H_2}(y)} - \frac{b}{2F}\frac{x_{H_2O}^a(y)}{x_{H_2}(y)} \int_0^y I(y)\, dy\right)$$

(A.1)

or

$$\alpha(y) = -\frac{F}{bI(y)}\frac{\mathrm{d}}{\mathrm{d}y}\left(N_{H_2}^{in}\frac{x_{H_2O}^a(y)}{x_{H_2}(y)}\right)$$
$$+\frac{1}{2I(y)}\frac{\mathrm{d}}{\mathrm{d}y}\left(\frac{x_{H_2O}^a(y)}{x_{H_2}(y)}\int_0^y I(y)\,\mathrm{d}y\right) \tag{A.2}$$

Expanding the second term on the right-hand side, it follows that

$$\alpha(y) = -\frac{F}{bI(y)}N_{H_2}^{in}\frac{\mathrm{d}}{\mathrm{d}y}\left(\frac{x_{H_2O}^a(y)}{x_{H_2}(y)}\right) + \frac{\int_0^y I(y)\,\mathrm{d}y}{2I(y)}\frac{\mathrm{d}}{\mathrm{d}y}$$
$$\times\left(\frac{x_{H_2O}^a(y)}{x_{H_2}(y)}\right) + \frac{x_{H_2O}^a(y)}{2I(y)x_{H_2}(y)}\frac{\mathrm{d}}{\mathrm{d}y}\left(\int_0^y I(y)\,\mathrm{d}y\right) \tag{A.3}$$

Note that

$$\frac{\mathrm{d}}{\mathrm{d}y}\left(\int_0^y I(y)\,\mathrm{d}y\right) = I(y) \tag{A.4}$$

Therefore, Eq. (A.3) can be rewritten as

$$\alpha(y) = -\left(\frac{F}{bI(y)}N_{H_2}^{in} - \frac{\int_0^y I(y)\,\mathrm{d}y}{2I(y)}\right)\frac{\mathrm{d}}{\mathrm{d}y}\left(\frac{x_{H_2O}^a(y)}{x_{H_2}(y)}\right)$$
$$+\frac{x_{H_2O}^a(y)}{2x_{H_2}(y)} \tag{A.5}$$

References

[1] T.E. Springer, T.A. Zawodzinski, S. Gottesfeld, Polymer electrolyte fuel-cell model, J. Electrochem. Soc. 138 (1991) 2334.

[2] T. Okada, G. Xie, M. Meeg, Simulation for water management in membranes for polymer electrolyte fuel cells, Electrochim. Acta 43 (1998) 2141.

[3] T.V. Nguyen, R.E. White, A water and heat management model for proton-exchange-membrane fuel-cells, J. Electrochem. Soc. 140 (1993) 2178.

[4] D.M. Bernardi, M.W. Verbrugge, A mathematical-model of the solid–polymer–electrolyte fuel-cell, J. Electrochem. Soc. 139 (1992) 2477.

[5] M. Eikerling, Y.I. Kharkats, A.A. Kornyshev, Y.M. Volfkovich, Phenomenological theory of electro-osmotic effect and water management in polymer electrolyte proton-conducting membranes, J. Electrochem. Soc. 145 (1998) 2684.

[6] F. Meier, G. Eigenberger, Transport parameters for the modelling of water transport in ionomer membranes for PEM-fuel cells, Electrochim. Acta 49 (2004) 1731.

[7] T.F. Fuller, J. Newman, Water and thermal management in solid–polymer–electrolyte fuel-cells, J. Electrochem. Soc. 140 (1993) 1218.

[8] P. Staiti, Z. Poltarzewski, V. Alderucci, G. Maggio, N. Giordano, A. Fasulo, Influence of electrodic properties on water management in a solid polymer electrolyte fuel-cell, J. Appl. Electrochem. 22 (1992) 663.

[9] K.-H. Choi, D.-H. Peck, C.S. Kim, D.-R. Shin, T.-H. Lee, Water transport in polymer membranes for PEMFC, J. Power Sources 86 (2000) 197.

[10] G.J.M. Janssen, M.L.J. Overvelde, Water transport in the proton-exchange-membrane fuel cell: measurements of the effective drag coefficient, J. Power Sources 101 (2001) 117.

[11] C.Y. Wang, Fundamental models for fuel cell engineering, Chem. Rev. (Washington) 104 (2004) 4727.

[12] M.M. Mench, Q.L. Dong, C.Y. Wang, In situ water distribution measurements in a polymer electrolyte fuel cell, J. Power Sources 124 (2003) 90.

[13] M.M. Mench, C.Y. Wang, M. Ishikawa, In situ current distribution measurements in polymer electrolyte fuel cells, J. Electrochem. Soc. 150 (2003) A1052.

[14] X.G. Yang, N. Burke, C.Y. Wang, K. Tajiri, K. Shinohara, Simultaneous measurements of species and current distributions in a PEFC under low-humidity operation, J. Electrochem. Soc. 152 (2005) A759.

[15] X.M. Ren, S. Gottesfeld, Electro-osmotic drag of water in poly (perfluorosulfonic acid) membranes, J. Electrochem. Soc. 148 (2001) A87.

[16] T.A. Zawodzinski, C. Derouin, S. Radzinski, R.J. Sherman, V.T. Smith, T.E. Springer, S. Gottesfeld, Water-uptake by and transport through Nafion(R) 117 membranes, J. Electrochem. Soc. 140 (1993) 1041.

[17] T.A. Zawodzinski, T.E. Springer, J. Davey, R. Jestel, C. Lopez, J. Valerio, S. Gottesfeld, A comparative-study of water-uptake by and transport through ionomeric fuel-cell membranes, J. Electrochem. Soc. 140 (1993) 1981.

[18] T.F. Fuller, J. Newman, Experimental-determination of the transport number of water in Nafion-117 membrane, J. Electrochem. Soc. 139 (1992) 1332.

[19] T.A. Zawodzinski, T.E. Springer, F. Uribe, S. Gottesfeld, Characterization of polymer electrolytes for fuel-cell applications, Solid State Ionics 60 (1993) 199.

[20] X. Ye, C.Y. Wang, Measurements of water transport properties through membrane electrode assemblies. Part I. Membranes, J. Electrochem. Soc., submitted for publication.

[21] T.A. Zawodzinski, J. Davey, J. Valerio, S. Gottesfeld, The water content dependence of electro-osmotic drag in proton-conducting polymer electrolytes, Electrochim. Acta 40 (1995) 297.

[22] S. Gottesfeld, T.A. Zawodzinski, in: C. Tobias (Ed.), Advances in Electrochemical Science and Engineering, vol. 5, Wiley and Sons, New York, 1997.

[23] G.Q. Lu, F.Q. Liu, C.Y. Wang, An approach to measuring spatially resolved water crossover coefficient in a polymer electrolyte fuel cell, J. Power Sources, doi:10.1016/j.jpowsour.2006.10.035.